

GEODETTIC OBSERVATIONS OF POSTSEISMIC DEFORMATION  
AROUND THE NORTH END OF SURFACE RUPTURE

By

John O. Langbein, M. J. S. Johnston, and A. McGarr,  
U.S. Geological Survey

Separate print from  
U.S. GEOLOGICAL SURVEY PROFESSIONAL PAPER 1254

The Imperial Valley, California,  
Earthquake of October 15, 1979

1982 .  
United States Government Printing Office

GEODETIC OBSERVATIONS OF POSTSEISMIC DEFORMATION  
AROUND THE NORTH END OF SURFACE RUPTURE

By

John O. Langbein, M. J. S. Johnston, and A. McGarr,  
U.S. Geological Survey

Separate print from  
U.S. GEOLOGICAL SURVEY PROFESSIONAL PAPER 1254

The Imperial Valley, California,  
Earthquake of October 15, 1979

1982  
United States Government Printing Office

# GEODETIC OBSERVATIONS OF POSTSEISMIC DEFORMATION AROUND THE NORTH END OF SURFACE RUPTURE

By JOHN O. LANGBEIN, M. J. S. JOHNSTON, and A. MCGARR,  
U.S. GEOLOGICAL SURVEY

## CONTENTS

Abstract .....	205
Introduction .....	205
Observations .....	207
Discussion .....	207
Conclusions .....	212
Acknowledgments .....	212
References cited .....	212

## ABSTRACT

We have measured postseismic deformation, using an electronic distance-measuring instrument, in the area around the northern third of observed surface rupture from the 1979 Imperial Valley earthquake. Measurement of a geodetic network consisting of 54 base lines was initiated on October 27, 1979, and the lines were repeatedly measured during the next several months. We analyzed the line-length changes in terms of a simple model of uniform slip over a semi-infinite plane, corresponding to the Imperial fault, and homogeneous strain changes in the surrounding region. For the interval October 27–December 13, 1979, the average rate of fault slip was found to be  $1.08 \pm 0.08$  mm/d, and the most significant component of strain change was an east-westward contraction of  $0.08 \pm 0.02$  microstrain per day, with an uncertainty of  $28.5^\circ$  in the azimuth of this component of the principal strain. Generally, the rate of postseismic deformation decreased over time during the entire period of observation. For example, from October 27 to November 14 the average rate of fault displacement was  $1.96 \pm 0.29$  mm/d, whereas from November 12 to December 13 the rate was  $0.80 \pm 0.13$  mm/d. From October 27 to November 14 the strain change was correspondingly rapid, with northwest-southeastward compression occurring at a rate of  $0.3 \pm 0.1$  microstrain per day. Most of these observations can be tentatively explained in terms of strain release on either side of the fault due to postseismic slip.

## INTRODUCTION

In this report we describe the preliminary results of a geodetic survey in the vicinity of the northern section of the Imperial fault after the main shock of October 15, 1979. On the basis of information of continuing postseismic fault motion of as much as 10 mm/d (P. W. Harsh, oral commun., 1979), we initiated a program of line-length measurements, using a Hewlett-Packard 3800A distance-measuring instrument and an array of

18 corner-cube reflectors. With this instrumentation, apparent strain changes along lines of about 2 km can be resolved at about the 2-microstrain level (Lisowski and Prescott, 1981).

Of particular interest with regard to questions of postseismic-strain redistribution was the area around the north end of the Imperial fault break. Most of the aftershocks tended to occur there and on the adjacent echelon Brawley fault zone and the Superstition Hills fault (Johnson and Hutton, this volume). Indications of displacements on the San Andreas fault (Sieh, this volume) and on the Superstition Hills fault (Fuis, this volume) also suggest continuing deformation in this northern area. In view of these displacements and because of the existence of excellent geodetic control across the central section of the Imperial fault (Mason and others, 1979; Crook and others, this volume), we concentrated on measuring ground deformation in and near the north third of the zone of ground breakage (Sharp and others, this volume).

Beginning on October 27, we made repeated measurements of the line lengths of 54 base lines (fig. 149) extending northwestward from the earlier geodetic network set up in 1970 by the Imperial College, London (Mason and others, 1979). Our new network includes three of the Imperial College bench marks (J33, G33, and G34), and six alignment-array bench marks (here designated HSE1, HSE3, HSW1, HSW3, HSW3', and HSW4), installed by Harsh (this volume) on either side of the fault at Harris Road (fig. 149). To avoid losing time in establishing this new network, we elected to use concrete nails driven into the road pavement as bench marks rather than more permanent marks, such as those used by Mason and others (1979).

As seen on the map (fig. 149), the network includes both lines that cross the fault and lines completely to the northeast or southwest of the trace. The geometry of the network was influenced largely by the availability of lines of sight across rather flat topography; thus the majority of lines follow roads. Another limitation on the network, imposed by the instrument used, was difficulty in measuring line lengths longer than 3 km.

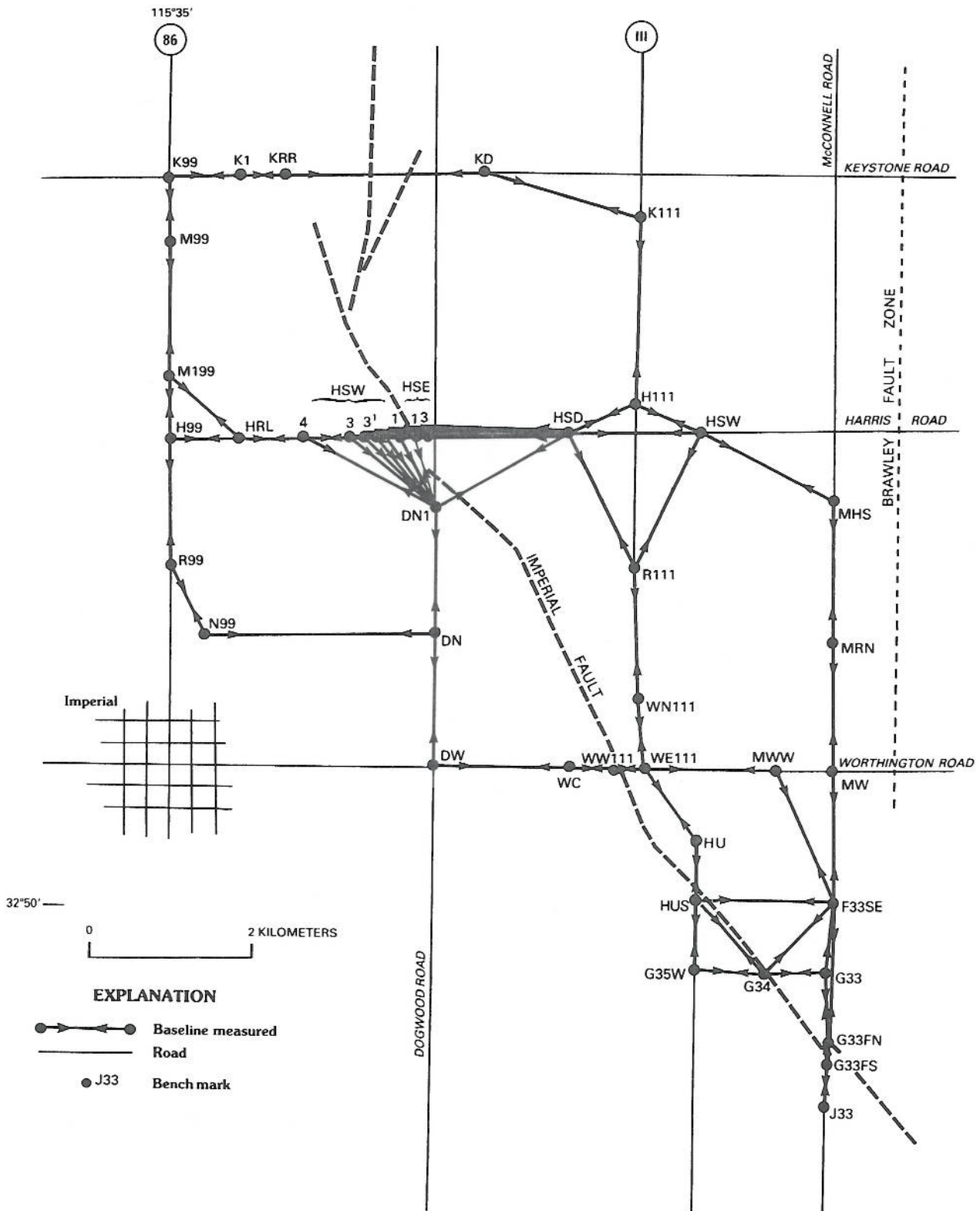


FIGURE 149.—Locations of base lines in geodetic network used to measure surface strain and slip on Imperial fault. Heavy dashed line indicates approximate location of observed trace of Imperial fault; light dashed line indicates Brawley fault zone. Obvious surface ruptures from October 15 earthquake could be observed north and south of Keystone Road.

As discussed below, the large number of lines allowed the determination of fault displacement and strain change as a function of time and position within the network. The capability of measuring deformation within regions of the network is important here because within the network the coseismic fault displacements exhibited spatial gradients to the southeast of Keystone Road of more than 2 mm/km across 10 km of the most obvious surface rupture. In the first 10 days after rupturing, postseismic fault displacements also showed a spatial gradient of more than 1 mm/km across the same rupture zone (Harsh, this volume; Sharp and others, this volume). Therefore, strain in this area should not be expected to be homogeneous.

**OBSERVATIONS**

Figure 150 plots the changes in line length for each base line in the network during the interval October 27–December 16, 1979. The time scales of these plots are somewhat longer than necessary because we intended to continue our observational program into the first quarter of 1980. Figure 150A shows the changes in displacement for only those lines that cross the surface trace of the Imperial fault; all other displacement-time histories are for lines that do not cross the fault. All data have been corrected for the effects of temperature, pressure, and humidity on the atmospheric refractive index (Bomford, 1971), and for shifts in the frequency of the reference oscillator of the instrument due to changes in ambient temperature (Lisowski and Prescott, 1981).

For the base lines that cross the fault, the line-length changes are apparently rapid and generally linear, although the displacement rate seems to decrease somewhat over time. On most of the base lines that do not cross the Imperial fault, changes in line length appear to be more subtle and of varying significance. The multitude of measured lines, however, provide considerable redundancy, and so good estimates of strain change can be made for selected regions of the network. The data from many base lines that do not cross the fault also indicate a standard deviation in the measurements smaller than the 4.5 mm estimated by Lisowski and Prescott (1981). For example, five base lines in our network were measured at least six times. Fitting linear trends to this data set gives estimates of the unbiased standard deviation of the fit of from 2.6 to 3.6 mm. Adding the data from the base lines measured five times gives an average standard deviation of 3.9 mm for fitting either a linear trend or a simple mean to the data. Estimates of the error in the atmospheric-refractive-index correction (Bomford, 1971) are assumed to be one part in 10<sup>6</sup>, which is statistically added to the 3.9-mm nominal error.

**DISCUSSION**

Although the observed fault displacements indicate that inhomogeneous strain change within the survey network is likely, it seemed worthwhile first to analyze the geodetic data in terms of a simple model involving constant fault slip and homogeneous deformation. In this report we elaborate this initial analysis by considering homogeneous deformation within regions of the network, but do not discuss more complex models involving finite faults.

Assuming an infinite fault with uniform slip in a half-space, we can use the observed line-length changes to infer the value of fault slip and the changes in the three horizontal components of strain. The degree of misfit to the resulting solution gives some indication of how useful our observations are likely to be if we were to analyze them in terms of more realistic fault models.

For an assumed homogeneous deformation, the changes in line length  $\Delta L_i$  are related to the slip rate  $\dot{U}$  and the components of the strain-rate tensor  $\dot{E}_{ee}$ ,  $\dot{E}_{en}$ , and  $\dot{E}_{nn}$  by:

$$\begin{aligned} \Delta L_i &= L_{ij} - \bar{L}_i \\ &= (T_{ij} - \bar{T}_i) [\dot{U} \cos \alpha_i + L_i (\dot{E}_{ee} \cos^2 \phi_i \\ &\quad + 2\dot{E}_{en} \cos \phi_i \sin \phi_i + \dot{E}_{nn} \sin^2 \phi_i)], \end{aligned}$$

where  $L_{ij}$  is the distance on the  $i$ th base line measured at time  $T_{ij}$ ,  $\bar{L}_i$  and  $\bar{T}_i$  are the average distance and time, respectively,  $\phi_i$  is the angle between the  $i$ th base line and the direction east, and  $\alpha_i$  is the angle between the fault trace and the  $i$ th base line. We use the technique of weighted least squares to determine the model parameters from the data; the weights used are the squares of the reciprocal of the standard measurement error for each data point. In the following discussion we present the results for different spatial and temporal subsets of the data (fig. 151). Because we use a weighted-least-squares technique here, the standard deviation of the fit to the model is dimensionless, and the values less than unity indicate a good fit of the model to the data.

Using the entire data set, we infer the following:

$$\dot{U} = 1.08 \pm 0.08 \text{ mm/d,}$$

$$\dot{E}_1 = -0.08 \pm 0.02 \text{ microstrain per day,}$$

$$\dot{E}_2 = 0.02 \pm 0.02 \text{ microstrain per day,}$$

$$\theta_1 = \text{N. } 89.4^\circ \pm 28.5^\circ \text{ E,}$$

and

$$\sigma = 1.00 \text{ mm/mm,}$$

THE IMPERIAL VALLEY, CALIFORNIA, EARTHQUAKE OF OCTOBER 15, 1979

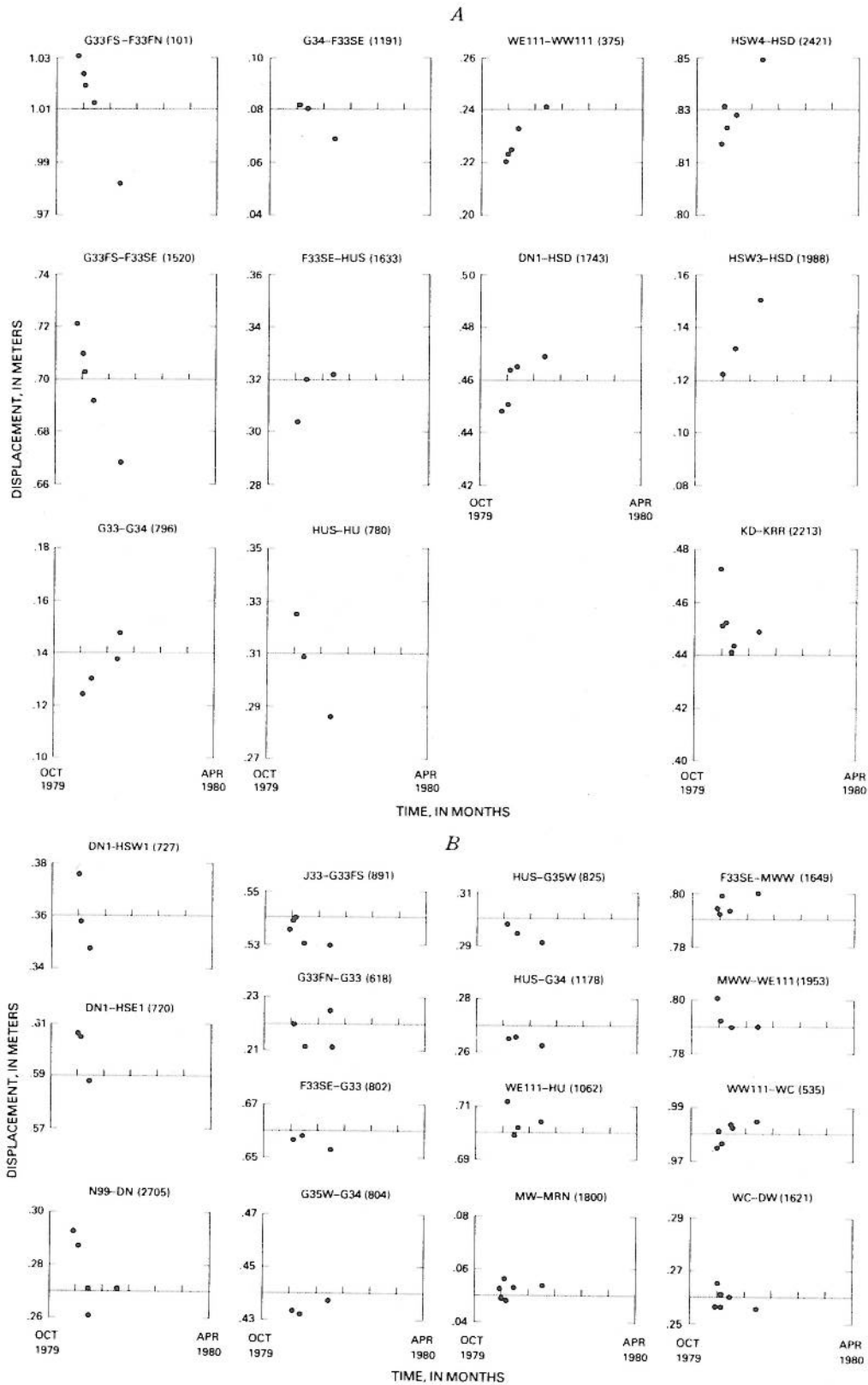


FIGURE 150.—Line length as a function of time for all base lines in geodetic network (see fig. 149 for locations). Each plot represents separate base line; number in parentheses following bench-mark names indicates length of base line (in meters). Time scale starts at October 1, 1979. *A*, Changes in displacement for only those lines that cross surface trace of Imperial fault. *B*, Changes in displacement for lines that do not cross Imperial fault.

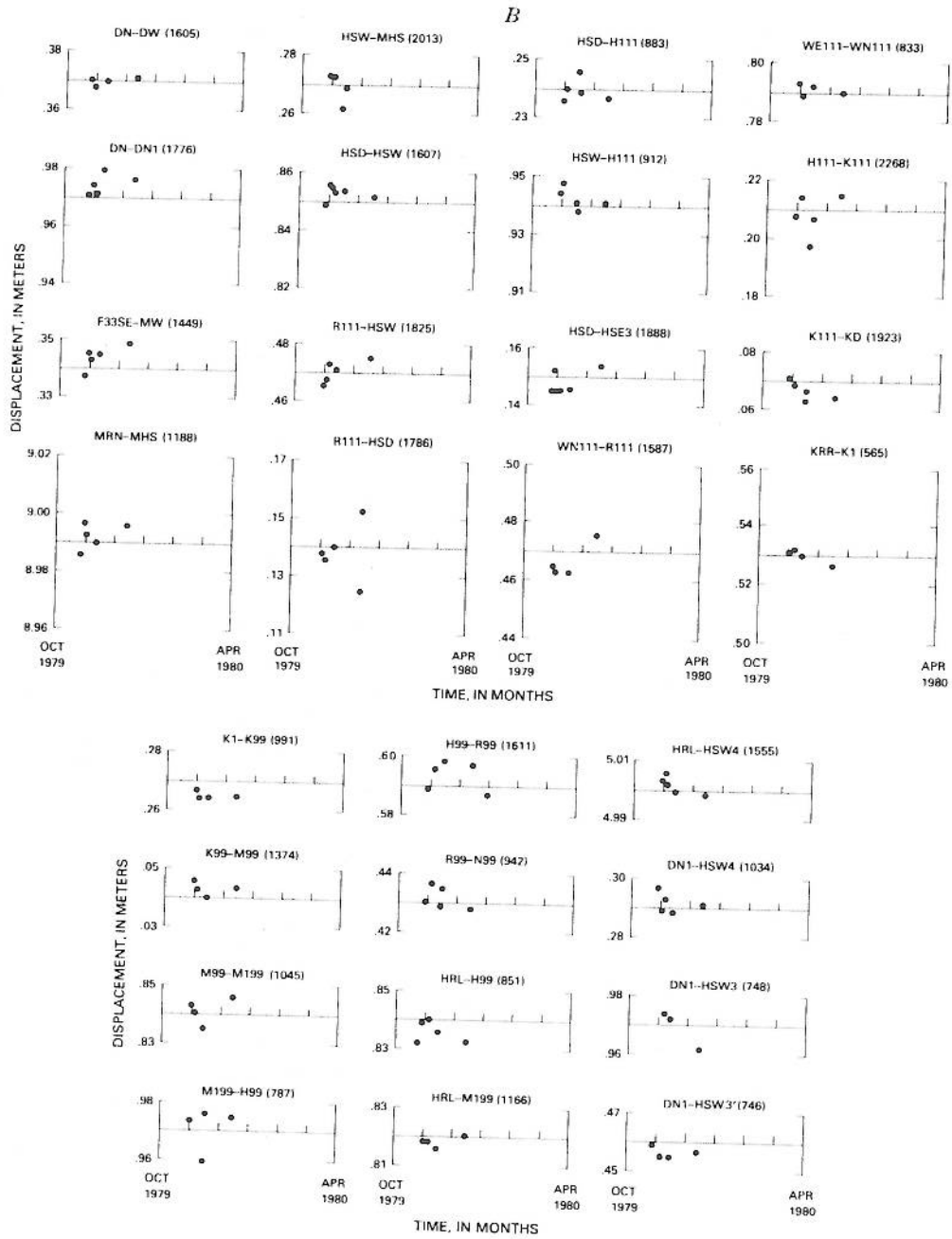


FIGURE 150.—Continued

ALL DATA

SUBSET (MEASUREMENT)	PERIOD		
	10/27-12/13	10/27-11/14	11/12-12/13
$\dot{E}_1$ ( $\mu$ str/d)	-0.07 ± 0.02	-0.32 ± 0.09	-0.05 ± 0.06
$\dot{E}_2$ ( $\mu$ str/d)	0.02 ± 0.02	0.07 ± 0.11	0.07 ± 0.06
$\theta^1$ azimuth	N.89° ± 22°E.	N.59° ± 10°W.	N.64° ± 21°E.
$\dot{U}$ (mm/d)	1.08 ± 0.08	1.96 ± 0.29	0.80 ± 0.13
$\sigma$ (mm/mm)	1.04	0.83	0.79
Number of observations	224	184	119
Vectors			

REGION II DATA

SUBSET (MEASUREMENT)	PERIOD		
	10/27-12/13	10/27-11/14	11/12-12/13
$\dot{E}_1$ ( $\mu$ str/d)	-0.10 ± 0.10	-0.11 ± 0.40	-0.04 ± 0.12
$\dot{E}_2$ ( $\mu$ str/d)	0.06 ± 0.10	-0.44 ± 0.41	0.22 ± 0.13
$\theta^1$ azimuth	N.71° ± 38°E.	N.63° ± 50°W.	N.89° ± 51°E.
$\dot{U}$ (mm/d)			
$\sigma$ (mm/mm)	0.68	0.61	0.75
Number of observations	34	26	17
Vectors			

EASTERN-BLOCK DATA

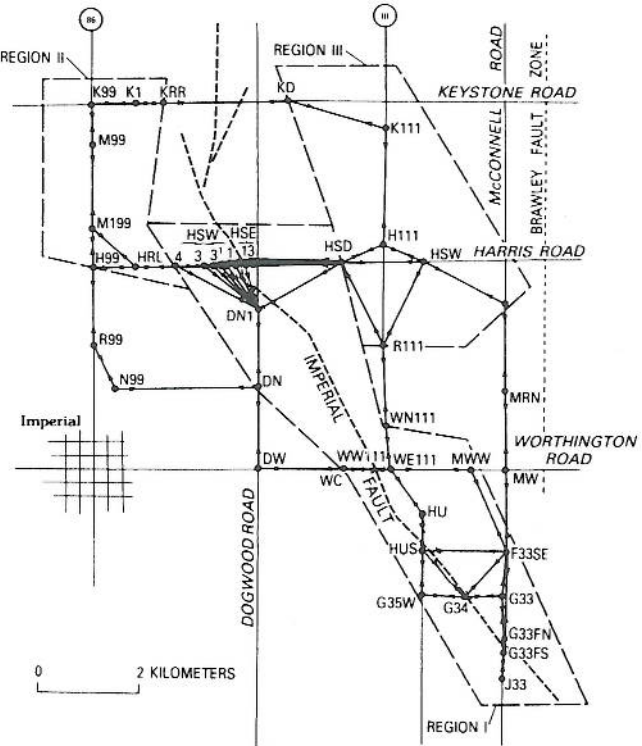
SUBSET (MEASUREMENT)	PERIOD		
	10/27-12/13	10/27-11/14	11/12-12/13
$\dot{E}_1$ ( $\mu$ str/d)	-0.06 ± 0.05	-0.27 ± 0.15	-0.00 ± 0.08
$\dot{E}_2$ ( $\mu$ str/d)	0.10 ± 0.05	0.19 ± 0.15	0.11 ± 0.06
$\theta^1$ azimuth	N.63° ± 14°W.	N.49° ± 9°W.	N.84° ± 45°E.
$\dot{U}$ (mm/d)			
$\sigma$ (mm/mm)	0.85	0.65	0.85
Number of observations	90	70	45
Vectors			

REGION III DATA

SUBSET (MEASUREMENT)	PERIOD		
	10/27-12/13	10/27-11/14	11/12-12/13
$\dot{E}_1$ ( $\mu$ str/d)	-0.07 ± 0.06	0.21 ± 0.18	-0.07 ± 0.10
$\dot{E}_2$ ( $\mu$ str/d)	0.08 ± 0.05	-0.28 ± 0.18	0.13 ± 0.09
$\theta^1$ azimuth	N.67° ± 16°W.	N.54° ± 13°E.	N.85° ± 30°E.
$\dot{U}$ (mm/d)			
$\sigma$ (mm/mm)	0.95	0.64	1.07
Number of observations	40	32	21
Vectors			

WESTERN-BLOCK DATA

SUBSET (MEASUREMENT)	PERIOD		
	10/27-12/13	10/27-11/14	11/12-12/13
$\dot{E}_1$ ( $\mu$ str/d)	-0.11 ± 0.07	-0.41 ± 0.21	-0.06 ± 0.12
$\dot{E}_2$ ( $\mu$ str/d)	0.04 ± 0.07	0.09 ± 0.21	0.12 ± 0.12
$\theta^1$ azimuth	N.65° ± 20°W.	N.65° ± 19°W.	N.47° ± 15°W.
$\dot{U}$ (mm/d)			
$\sigma$ (mm/mm)	0.88	0.84	0.62
Number of observations	98	76	49
Vectors			



REGION I DATA

SUBSET (MEASUREMENT)	PERIOD		
	10/27-12/13	10/27-11/14	11/12-12/13
$\dot{E}_1$ ( $\mu$ str/d)	-0.10 ± 0.08	0.28 ± 0.23	0.08 ± 0.10
$\dot{E}_2$ ( $\mu$ str/d)	0.06 ± 0.08	-0.55 ± 0.23	-0.24 ± 0.10
$\theta^1$ azimuth	N.46° ± 12°E.	N.50° ± 7°E.	N.58° ± 11°W.
$\dot{U}$ (mm/d)	0.99 ± 0.10	1.75 ± 0.30	0.73 ± 0.14
$\sigma$ (mm/mm)	1.18	0.91	0.74
Number of observations	110	83	56
Vectors			

FIGURE 151.—Results of estimating slip and strain rates for different data subsets.  $U$  is value of right-lateral slip, and  $E_1$ ,  $E_2$ , and " $\theta^1$ " azimuth are values of principal strain components and its axis. Vectors indicate azimuth and magnitude of principal strains; direction north points vertically upward on the page. Inset shows locations of regions I, II, and III within network (see fig. 149 for detail). Western and eastern blocks refer to Imperial fault.

where  $\theta_1$  is the azimuth of the principal strain rate  $\dot{E}_1$ , and  $\sigma$  is the standard deviation of the fit of the model to the data. Besides the high rate of fault slip, the major finding from these data is an east-westward contraction at a rate of 0.08 microstrain per day, four times larger than its corresponding estimate of the standard error. We note that the actual direction of contraction is poorly determined. The fit of this model to the data, as indicated by the normalized standard deviation  $\sigma$ , is surprisingly good in view of our simplifying assumptions of uniformity in strain and fault slip in both space and time.

The data from the entire network can be subdivided into two intervals (fig. 151): the first from the initial survey to the survey in mid-November, and the second from mid-November to mid-December. For the first interval the slip rate averaged  $1.96 \pm 0.29$  mm/d, and for the second interval the data indicate a lower slip rate of  $0.80 \pm 0.13$  mm/d. Another significant measurement for the first interval is the contraction rate of  $0.32 \pm 0.12$  microstrain per day along a northwesterly azimuth. The strain rates for the second interval, however, do not differ significantly from zero (fig. 151)—a result to be expected if the rate of deformation was decreasing over time.

Northwest-southeastward contraction also appears to be significant in the areas either to the west or to the east of the Imperial fault (fig. 151) during the first interval. For the entire period of observation, the strain rates in the western block agree well with those inferred from the entire data set. Thus, insignificant strain changes during the second interval and southeast-northwestward contraction during the first interval are evident in both sets of data. Similar conclusions, however, are not substantiated by the data from the eastern block. In contrast to the changes during the first interval, significant strain changes occurred in this block during the second interval. Significant north-southward extension during the second interval, in conjunction with strain changes during the first interval that show nearly pure shear, indicates 0.10 microstrain per day of northeast-southwestward extension over the entire period of observation.

We note that the observation of northwest-southeastward contraction during the first interval in all the data is consistent with strain release due to right-lateral slip on the Imperial fault (Scholz and Fitch, 1969). As pointed out above, problems encountered by using this simple, uniform-strain interpretation may arise as a result of the need to consider: (1) the likely nonuniform distribution of slip; (2) the effect of sympathetic slip on the Brawley fault zone and the Superstition Hills fault to the east and west of the network, respectively; and (3) such geometric effects as the change in fault strike near Harris Road, which may be

associated with a substantial vertical component of faulting on this section of the Imperial fault, as observed by Sharp and Lienkaemper (this volume).

In an attempt to determine the spatial variations in strain within the network, we divided the survey area into three smaller regions (inset, fig. 151) to allow internal comparison. As expected, estimates of strain were not so well determined because of the fewer measurements available. Region I consists of all the base lines that cross the Imperial fault south of Keystone Road and those base lines that are within 1.5 km of the fault. Both the inferred slip and strain rates in this region apparently decrease over time, and the strain during the first interval indicates primarily north-west-southeastward contraction. A curious feature is an apparent rotation of the principal strains during the second interval. Region II consists of the base lines on the west side of the Imperial fault near the terminus of the surface rupture. We note a compressional trend, but it is only marginally significant for the first interval, when the slip rate was high. This pattern of strain, in which the estimated strain exceeds the standard deviation, is consistent with simple dislocation models that predict contraction in this northwestern lobe with slip on a right-lateral fault. The significant north-southward extension observed in this region during the second interval is unexplained at this time. Region III consists of the base lines near Harris Road and State Highway 111. Again, significant northwest-southeastward contraction occurred during the first interval, and north-southward extension during the second.

The leveling data of Sharp and Lienkaemper (this volume) indicate that the postseismic fault displacement was mostly dip-slip. Figure 152 plots the relative uplift of the west side of the fault at Harris Road, along with some of our corresponding horizontal measurements. Except for the measurements along base line

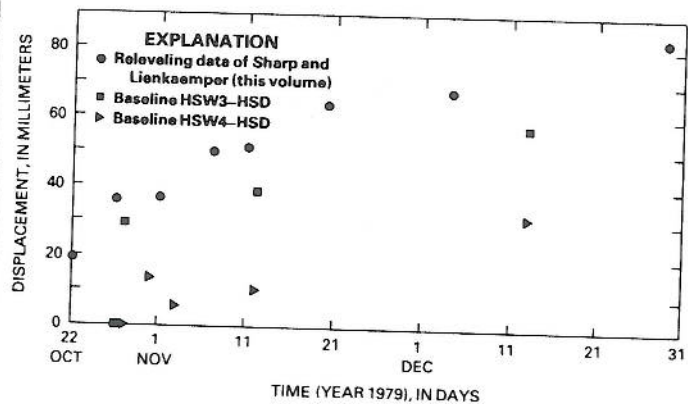


FIGURE 152.—Uplift of western block of Imperial fault relative to eastern block at Harris Road (see fig. 149 for location), from leveling data of Sharp and Lienkaemper (this volume). Horizontal data from our network around Harris Road are also plotted at same scale.

HSW3 to HSD made on October 27, the plot of the vertical and horizontal data (fig. 152) seems to indicate a similar history of deformation. We can determine the dip of the Imperial fault near Harris Road, at least in principle, by comparing the vertical and extensional components of the fault-displacement vector. We first attempted to determine the horizontal component of the slip vector from measurements along Harris Road and from bench mark DN1 (fig. 149) crossing the area of interest, but these data were inadequate to estimate both horizontal components. Our data were well suited, however, to estimate the projection of the horizontal-slip vector along Harris Road, which is probably the most significant component in terms of an estimate of the local fault dip because the fault strikes nearly north-south in this locality (Sharp and others, this volume). Accordingly, we compare the line-lengthening rates over the base lines extending from bench mark HSD with the releveling data of Sharp and Lienkaemper (this volume) (fig. 152), to infer an apparent eastward dip of  $49^{\circ} \pm 5^{\circ}$  E. which agrees well with field measurements of dip near Harris Road indicating an eastward dip of  $59^{\circ} \pm 8^{\circ}$  E. (R. V. Sharp and M. G. Bonilla, oral commun., 1980).

### CONCLUSIONS

Postseismic geodetic-strain changes obtained in the area around the north end of the Imperial fault rupture display considerable spatial and temporal complexity. As a first step in analyzing these data, we used a simple model consisting of uniform slip and strain to fit the data. Although many problems remain, the initial fit is surprisingly good and allows two general conclusions to

be drawn. (1) Significant postseismic fault displacement can easily be detected with this technique, using all fault-crossing lines; the rate of fault slip decreases over time. (2) Significant changes in strain, observed within about a 3-km zone on either side of the fault, were mainly characterized by a northwest-southeastward compression of 0.3 microstrain per day during the first 2 weeks after initial measurements were made.

### ACKNOWLEDGMENTS

The surveys were performed using equipment kindly loaned us by J. C. Savage, W. H. Prescott, Michael Lisowski, and A. G. Lindh, all of the U.S. Geological Survey; R. Estes of the Imperial County Public Works Department; and Mr. Parker of Parker and Riddle, Inc., El Centro, Calif. J. E. Estrem provided field assistance during the initial survey, and P. W. Harsh supplied bench marks and other equipment for the field operations.

### REFERENCES CITED

- Bomford, Guy, 1971, *Geodesy* (3d ed.): London, Oxford University Press, 731 p.
- Lisowski, Michael, and Prescott, W. H., 1981, Short-range distance measurements along the San Andreas fault system in central California, 1975 to 1979: *Seismological Society of America Bulletin*, v. 71, no. 5, p. 1607-1624.
- Mason, R. G., Brander, J. L., and Bill, M. G., 1979, Mekometer measurements in the Imperial Valley, California, in Whitten, G. A., Green, Ronald, and Meade, B. K., eds., *Recent crustal movements, 1977: Tectonophysics*, v. 52, no. 1-4 (special issue), p. 497-503.
- Scholz, C. H., and Fitch, T. J., 1969, Strain accumulation along the San Andreas fault: *Journal of Geophysical Research*, v. 74, no. 27, p. 6649-6666.